American Mineralogist, Volume 86, pages 1380–1386, 2001

High-pressure behavior of clinochlore

MARK D. WELCH[1,*] AND WILLIAM G. MARSHALL[2]

[1]Department of Mineralogy, The Natural History Museum, Cromwell Road, London, SW7 5BD, U.K.
[2]ISIS Facility, Rutherford Appleton Laboratory, Chilton, Didcot, Oxon OX11 0QX, U.K.

ABSTRACT

The room-temperature bulk modulus of synthetic end-member clinochlore, $Mg_5AlSi_3AlO_{10}(OD)_8$, has been determined in the pressure range 0 to 6.5 GPa using neutron powder diffraction: K_0 = 75.4(2.7) GPa, K_0' = 4; K_0 = 72.3(2.4) GPa, K_0' = 5.4(1.0). A structural comparison is made with the related mineral brucite, $Mg(OH)_2$. Clinochlore is a much stiffer structure than brucite (K_0 = 41 – 47 GPa). Both minerals have very similar in-plane compressions of their polyhedral sheets and so their very different bulk moduli arise from different compressibilities normal to the structural layering. Rietveld refinements of neutron-diffraction data for clinochlore collected at 0, 1.2, 2.5, and 4.7 GPa reveal that compression normal to the layering is equally partitioned between the interlayer and the 2:1 layer; the octahedral sheets of the brucite-like and 2:1 layers are uncompressed to 4.7 GPa. Increasing pressure strengthens the H3(D3)···O3 hydrogen bond, which contracts linearly from 1.88(2) Å at 0 GPa to 1.77(2) Å at 4.7 GPa, possibly with a concomitant lengthening of the O6-H3(D3) hydroxyl bond from 1.05(2) Å to 1.10(2) Å over the same pressure range.

INTRODUCTION

Studies of the effects of high pressure upon hydrogenous components of minerals are relevant to developing realistic models of the physical behavior of mantle rocks. Defining correlations between H environment, hydrogen-bond lengths and angles, and their spectroscopic expression allows the behavior of hydrogenous components to be studied at high pressure by vibrational spectroscopy. Diffraction studies play a major role in achieving this objective.

Chlorite is a major constituent of hydrated oceanic crust and may be significant as a carrier of water deep into cold subduction zones (Peacock 1990). Hence, the structural behavior of chlorite at high pressure, particularly how its hydrogenous components affect its compressibility, is relevant to mantle geophysics. High-pressure chlorites, including those originating in the upper mantle, have compositions close to that of end-member clinochlore, $Mg_5AlSi_3AlO_{10}(OH)_8$. In hot subduction zones, iron-bearing chlorites of the oceanic crust break down and release water into the overlying mantle wedge. The conditions in the mantle wedge are well within the known stability field of clinochlore, where the latter is expected to be the major aluminous phase in low-alkali hydrous peridotites (Jenkins 1981). Hence, there is the possibility that chlorite is "recycled" in subduction zones and, therefore, is likely to be a major player in the water budget of the upper mantle in these regions.

Chlorite presents difficulties for high-pressure, single-crystal X-ray diffraction studies because natural crystals usually have considerable fine-scale stacking disorder (monoclinic/ triclinic intergrowths), and synthetic chlorite crystals are too small and too highly aggregated for such studies. Streaking of reflections parallel to **c*** arising from stacking disorder leads to a poorly constrained *c* parameter (e.g., Hazen and Finger 1978) and is the main reason why the equation of state of chlorite has not been reliably determined. In this case, powder diffraction can provide valuable information on the high-pressure behavior of chlorite, provided that high-quality synthetic material is available. Synthetic monoclinic (*C*2/*m*) clinochlore grown at 1.4–1.5 GPa and 740–780 °C is stoichiometric, well-crystallized, and free of stacking disorders (Jenkins and Chernosky 1986; Welch et al. 1995; Baker and Holland 1996). In this paper we present the results of a high-pressure study of synthetic end-member *C*2/*m* clinochlore by neutron powder diffraction. The equation-of-state (EoS) of this chlorite has been determined to 6.5 GPa, and information on the role of interlayer hydrogen bonding in the compressional behavior has been obtained. Neutrons are scattered much more strongly by protons than are X-rays and so neutron diffraction is very well-suited to studying proton behavior.

Chlorite structure

The structure of chlorite is shown in Figure 1. It comprises alternating layers of brucite-like (B) and talc-like (2:1) structure. Interlayer bonding involves only hydrogen bonds; one-third of the atoms in chlorite are involved in hydrogen bonding, and it is this major structural feature that is the subject of the present study. The long- and short-range cation-ordering behavior of chlorites is now well understood from recent X-ray and spectroscopic studies (e.g., Rule and Bailey 1987; Welch et al. 1995; Smyth et al. 1997), which have shown that $^{[6]}$Al is at M4 and $^{[6]}$Mg is ordered at M3 (M3:M4 = 2:1). In end-member clinochlore, M1 and M2 sites of the 2:1 layer are filled by $^{[6]}$Mg. A ^{29}Si MAS NMR study of synthetic monoclinic (*C*2/*m*) end-member clinochlore by Welch et al. (1995) showed that there is a high degree of Al-Si short-range order within the tetrahedral sheet, as is also found in phlogopite and related micas (Herrero et al. 1987; Circone et al. 1991). *C*2/*m* clinochlore has only one crystallographically distinct tetrahedral site with an average occupancy of 0.75Si + 0.25Al. The

* E-mail: mdw@nhm.ac.uk

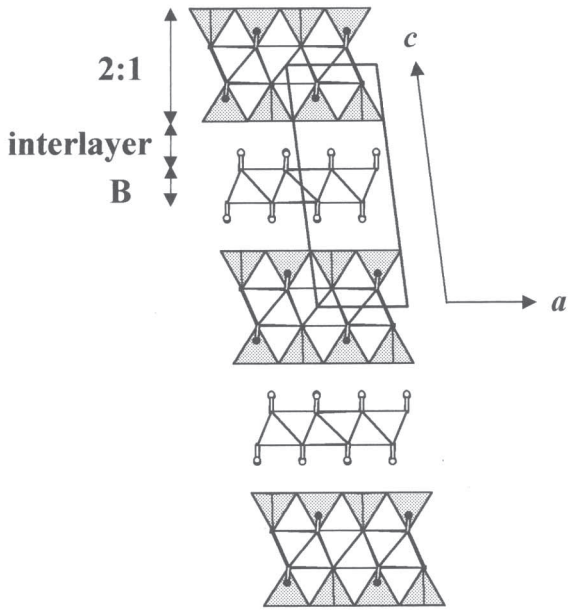

FIGURE 1. Structural layering of chlorite. There are two interlayers per *c* repeat. Hydrogen bonds form between the hydroxyl protons of the B layer and the basal-oxygen atoms of the tetrahedral sheet.

cation-ordering behavior outlined above is supported by a recent phase-equilibrium and thermochemical study of chlorite stability (Baker and Holland 1996).

Hydrogen-bonding topology

The hydrogen-bonding topologies of the room-temperature structures of brucite (Catti et al. 1995) and clinochlore (Joswig et al. 1989) are compared in Figure 2. The two topologies are very different: brucite has a trifurcated hydrogen bond 2.5 Å long, whereas clinochlore has local O-H···O groupings without any H sharing between acceptors. The hydrogen-bonds are much shorter in clinochlore (1.9 to 2 Å) than in brucite. There are also vacant sites within the sheets of basal O atoms of the tetrahedral layer. Consequently, it is of interest to see what differences in the compressional behavior of clinochlore and brucite may arise from their very different hydrogen-bonding topologies.

EXPERIMENTAL PROCEDURES

Sample synthesis and characterization

A total of 0.41g of deuterated clinochlore was synthesized on composition from a gel ($5MgO{\cdot}Al_2O_3{\cdot}3SiO_2$) in seven experiments at 1.5 GPa, 690–730 °C, 4–5 days, in a piston-cylinder apparatus using a 0.75 inch NaCl pressure cell. This gel and the experimental conditions used were the same as those used by Welch et al. (1995) in their NMR study. Deuterium was added as D_2O (99.9% D, Aldrich Chemicals). Exactly the same pressurization-heating-depressurization-cooling route was used in each synthesis to achieve sample constancy. Each product was examined by optical microscopy and X-ray powder diffraction to check for purity and composition. All products were monophase clinochlore. The *c* parameter of chlorite is a sensitive index of composition, and a well-established correlation based upon X-ray data exists between *c* and Al content

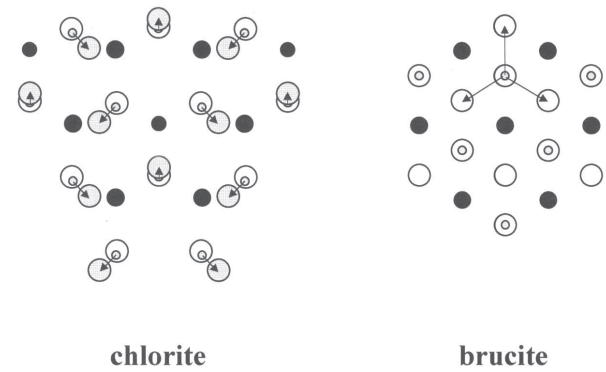

FIGURE 2. Hydrogen-bonding topologies of chlorite and brucite. Cations are solid black circles (Mg large), hydrogens are small gray circles, hydroxyl O atoms are white circles and basal-oxygen atoms (chlorite only) are large gray circles. Arrows indicate hydrogen bonds and point from the proton to the O atom acceptor. All hydrogen bonds are shown for chlorite; for clarity only a single trifurcated hydrogen bond is shown for brucite. The hydrogen-bond distances at room temperature and pressure are 1.9 to 2 Å for chlorite and 2.5 Å for brucite.

(Baker and Holland 1996): $X[AlAlMg_{-1}Si_{-1}] = 4(14.642 - c)$, displaced from the fictive chlorite end-member $Mg_6Si_4O_{10}(OH)_8$ by *X*; end-member clinochlore has $X = 1$. Unit-cell refinements using X-ray powder diffraction with an external NBS Si standard indicate that the average *c* parameter for the seven samples is 14.395(8) Å. The seven samples were then mixed together for the neutron experiment; *c* determined by X-ray powder diffraction for the bulk aggregate sample is 14.404(11) Å, corresponding to composition $X = 0.99(5)$, close to that of end-member clinochlore. The X-ray peak-widths for the bulk sample are only 0.03° wider than those of individual samples, implying that the bulk sample is homogenous.

Neutron diffraction experiments

Unlike X-ray diffraction, neutron diffraction is well-suited to studying the behavior of protons in inorganic materials as a consequence of the pseudo-random variation of neutron scattering length with atomic number. Deuterated samples were used in the present study so as to avoid the high background levels that result from the strong incoherent scattering from the proton. A further advantage of using D is that it is a stronger neutron scatterer than H. Calculated PEARL diffraction patterns for deuterated clinochlore and protonated clinochlore are significantly different, with the former having almost all of its scattering intensity below 3 Å, whereas the latter has several intense peaks above 3 Å. This difference turns out to be very advantageous for deuterated clinochlore because the background noise level increases markedly above 3 Å and can lead to lower-quality patterns that are difficult to refine satisfactorily. In what follows, we refer to deuterated clinochlore as "clinochlore" for brevity.

Two separate experiments were performed: (1) a pressure calibration to 6.5 GPa from which the equation of state (EoS) of clinochlore was obtained, and (2) a series of 8–12 h runs used to study the detailed effects of pressure upon the chlorite structure, particularly the hydrogen-bonding behavior. Both experiments used a Paris-Edinburgh pressure cell fitted with tungsten car-

bide anvils and a toroidal null-scattering TiZr alloy gasket (Nelmes et al. 1993). The initial sample-chamber volume is 90 mm^3. The whole assembly was loaded into the PEARL/HiPr diffractometer on beamline S9 at the ISIS pulsed-neutron spallation source, Rutherford Appleton Laboratory, U.K. This is a high-flux, medium-resolution diffractometer that is dedicated to high-pressure experiments. There are nine detector modules covering 83–97 °2θ, corresponding to a *d*-spacing range of 0.5–4.1 Å. The resolution $\Delta d/d$ over this range is 0.8%. In the standard configuration the incident beam enters through the back of the WC anvil and the diffracted beams exiting through the TiZr gasket are detected. Load was applied to the anvil and gasket assembly by means of the in situ hydraulic ram of the Paris-Edinburgh cell. For these particular experiments the hydraulic fluid was lubricating oil (ENERPAC grade HF95Y), with ram pressures being recorded to the nearest bar.

Fluorinert, a perfluorinated hydrocarbon mixture (grade used was FC75, supplied by 3M), was used as the pressure-transmitting medium in both experiments. For the EoS experiment, 0.160 g of clinochlore powder was mixed in an agate mortar with 0.068 g of dry NaCl (pressure standard) giving the usual 2:1 sample:NaCl volume ratio. The mixture was then slurried with fluorinert and pressed into a spheroidal pellet. For the structural study, 0.264 g of clinochlore powder was slurried with fluorinert but not pelletized.

RESULTS

Rietveld refinements

The structural model used for Rietveld refinement was based upon the ambient single-crystal neutron diffraction study of a natural Mg-rich clinochlore (*C*2/*m*) by Joswig et al. (1989). Site occupancies used the cation-ordering models of Bailey (1988) and Welch et al. (1995), based upon single-crystal X-ray and NMR studies, respectively: T = 0.25Al + 0.75Si, M1= M2 = M3 = Mg, M4 = Al. Starting atom coordinates used are those of Joswig et al. (1989). While chlorite is a complex structure compared with, say, brucite, its simple modular construction (discrete 2:1 and B layers) and well-known site occupancies allow initial refinement using a well-restrained model. (Mg,Al)-O, T-O, and O-D bond-lengths were allowed to vary within ± 0.04 Å, ± 0.02 Å and ± 0.1 Å of the Joswig et al. (1989) values, respectively. In the final stages of refinement all restraints were removed and satisfactory convergence to χ^2 values of between 1.3 and 1.8 was achieved for a total of 63 refined parameters (43 structural, 20 experimental).

In both the EoS and structural studies, the diffraction patterns were processed using the whole-pattern Rietveld refinement program GSAS (Larson & Von Dreele 1994). The high-pressure diffraction patterns contain contributions from the WC anvils and their Ni binder, and these contributions were included in the Rietveld refinements. In the case of the EoS data, where only unit-cell data for deuterated clinochlore and NaCl were sought, refinement was continued until convergence was achieved for the unit-cell parameters, scale factor, peak-shape and background parameters. Even without refining atomic coordinates, wR_p factors of 4% were readily achieved for the EoS data. Final wR_p values for the structural study were 2 to 3%.

EoS study

Pressures were calculated from the NaCl lattice constant using the room-temperature isotherm of the NaCl EoS of Decker (1971). Reported pressures are accurate to within 0.1 GPa. It is noteworthy that the fractional errors on cell parameters are small at <0.05%. The volume data for deuterated clinochlore were fit to second- and third-order Birch-Murnaghan EoSs of the general form:

$$P = 1.5K_0[(V_0/V_P)^{7/3} - (V_0/V_P)^{5/3}]\{1 + 0.75(K_0' - 4)[(V_0/V_P)^{2/3} - 1]\}$$

where K_0 is the bulk modulus and K_0' is its pressure derivative evaluated at zero pressure, V_0 is the ambient unit-cell volume and V_P is the unit-cell volume at higher pressure; $K_0' = 4$ for a second-order Birch-Murnaghan EoS. The 1σ errors on V_0/V_P values were calculated as defined in Bevington (1969) and are less than ± 0.001. Data were weighted by $1/\sigma^2$ for least-squares. The fitting to second- and third-order EoSs includes a pressure uncertainty of ± 0.1 GPa. An ambient (room *P* and *T*) data set was collected for the whole bulk sample, which was placed inside a vanadium can. The ambient unit-cell parameters are a = 5.332(1) Å, b = 9.224(2) Å, c = 14.414(2) Å, β = 97.07°, V = 703.50(16) $Å^3$. The c parameter value implies that X = 0.91(4), which is close to end-member. Within experimental error (c parameter), this value is the same as that determined by X-ray powder diffraction. The EoS data for clinochlore are given in Table 1 and cell parameters are plotted in Figure 3. The a and b parameters have nearly linear compressibilities to 6.5 GPa, whereas the c parameter is markedly non-linear. The variation of V_P/V_0 with pressure is shown in Figure 4 and is fit to second- and third-order Birch-Murnaghan EoSs. K_0 for the fit to a second-order EoS (K_0' = 4) is 75.4 ± 2.7 GPa, with R^2 = 0.99924. The fit to a third-order EoS gives K_0 = 72.3 ± 2.4 GPa and K_0' = 5.4 ± 1.0, with R^2 = 0.99971. The two fits are indistinguishable within error, implying that the highest pressure reached was not high enough to register distinct third-order behavior.

The second "ambient" unit-cell volume recorded when the pressure cell was returned to room pressure after the high-pressure experiment is 702.54(58) $Å^3$ and is in good agreement with the vanadium-can data, but suggests either a small residual pressure (<0.1 GPa) in the pressure cell or a slight hysteresis in the sample. Pressures for the structure-refinement runs were calculated from the K_0 = 75.4 GPa derived from a second-order fit to the EoS data.

Structure study

The experimental, refined, and difference patterns for clinochlore at 1.2 and 4.7 GPa are shown in Figure 5 and cell parameters are given in Table 1. Minor peak broadening due to non-hydrostatic stress is noticeable in the 4.7 GPa pattern, but this was easily modelled and did not affect the quality of the refinement. All four diffraction patterns from the structural study were refined to final wR_p values of less than 3%. The following parameter turn-on sequence was used: scale factors (clinochlore, WC, and Ni), background, peakshape unit-cell parameters, O *xyz*, D *xyz*, O U_{iso}, Mg *xyz*, $^{[6]}$Al *xyz*, T *xyz*, Mg, Al, Si U_{iso}, D U_{iso}. Atom coordinates, structural-layer spacings, and deuterium-oxygen distances are given in Tables 2, 3, and 4 re-

TABLE 1. Unit-cell parameters of clinochlore (*C*2/*m*) as a function of pressure at room temperature

P (GPa)*	*a* (Å)	*b* (Å)	*c* (Å)	β°	V_P (Å^3)	V_P/V_0
0 †	5.332(1)	9.224(2)	14.414(2)	97.07(2)	703.50(16)	1
0 ‡	5.338(3)	9.210(5)	14.407(7)	97.30(6)	702.54(58)	–
0.46	5.326(2)	9.207(3)	14.383(4)	97.38(4)	699.50(31)	0.9943(6)
1.15	5.311(2)	9.178(3)	14.327(4)	97.36(4)	692.67(31)	0.9846(6)
1.20	5.308(1)	9.186(2)	14.316(1)	97.27(2)	692.45(7)	–
1.63	5.300(2)	9.174(4)	14.298(4)	97.42(4)	689.45(34)	0.9800(7)
2.18	5.287(3)	9.159(5)	14.245(5)	97.35(6)	684.20(37)	0.9726(8)
2.46	5.283(1)	9.143(2)	14.220(1)	96.88(2)	681.84(7)	–
2.85	5.283(3)	9.123(6)	14.192(5)	97.23(7)	678.65(37)	0.9647(8)
3.73	5.267(3)	9.095(6)	14.148(5)	97.37(6)	672.11(37)	0.9554(8)
4.65	5.243(1)	9.068(2)	14.117(2)	97.38(3)	665.62(10)	–
5.25	5.245(3)	9.041(6)	14.053(5)	97.33(6)	660.86(38)	0.9394(8)
6.46	5.222(4)	9.018(7)	14.006(6)	97.24(8)	654.29(41)	0.9300(9)

* Uncertainty on P is ± 0.1 GPa data used in full structure refinement but not in EoS determination.
† Ambient vanadium-can data.
‡ Ambient in pressure-cell after decompression.

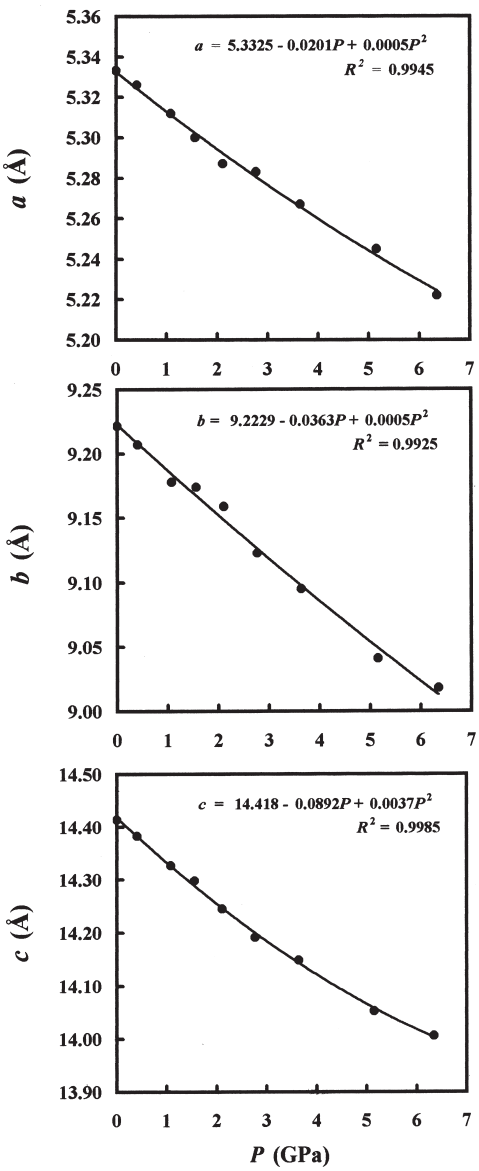

FIGURE 3. The *a*, *b*, and *c* parameters of clinochlore as a function of pressure. In each case the goodness-of-fit to a quadratic equation in *P* is indicated by the R^2 value.

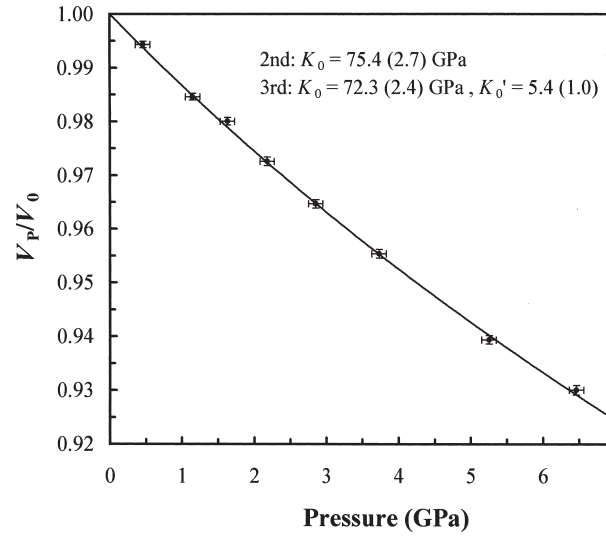

FIGURE 4. V_P/V_0 as a function of pressure, showing the fit a third-order Birch-Murnaghan EoS. The second- and third-order fits are almost identical and so only the third-order fit is shown. Errors on pressures are ±0.1 GPa. 2σ errors on V_P/V_0 are shown as error bars. The derived K_0 value for the second-order fit and the K_0 and K_0' values for the third-order fit are indicated.

spectively. Initially, a soft restraint was imposed on the O-D bond-length (within ± 0.1 Å of starting values), although, as we shall see, the result was very similar to that of the unrestrained refinement. Preferred orientation was refined, but essentially none was registered.

DISCUSSION

The room-temperature bulk modulus of clinochlore, 75 ± 3 GPa, is much higher than the values obtained by neutron powder diffraction for brucite of 47 ± 5 GPa (Parise et al. 1994) and 41 ± 2 GPa (Catti et al. 1995), indicating that clinochlore is a much stiffer structure. We now consider the contributions of the different structural layers of clinochlore to its compression. It will be useful in the discussion that follows if we now define layer thicknesses:

(1) Interlayer thickness: $(\Delta z_1)c\sin\beta$, where Δz_1 is the *smallest* difference in *z* coordinate for between brucite-layer O atoms and

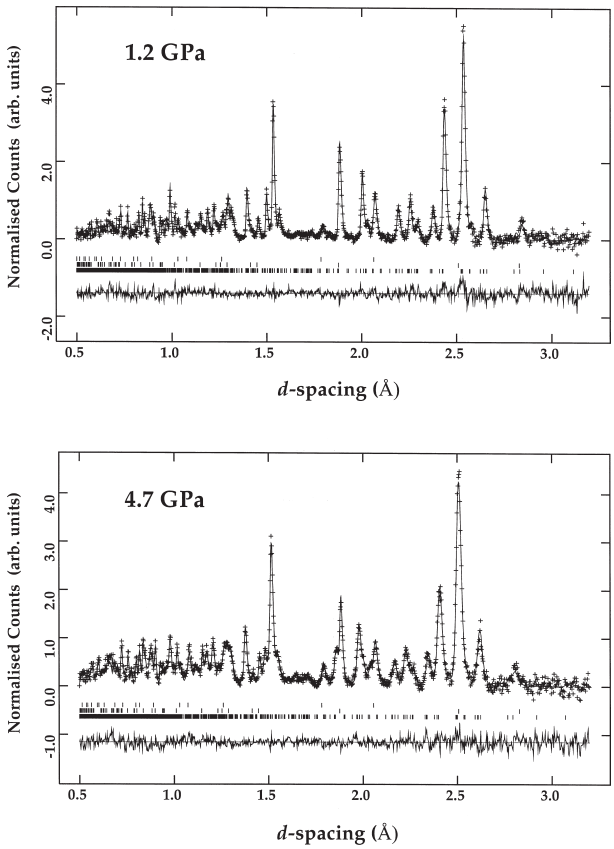

FIGURE 5. Experimental, calculated, and difference patterns for Rietveld refinements of the 1.2 and 4.7 GPa data. The three sets of refinement markers refer to WC (upper), Ni (middle), and clinochlore (lower).

basal O atoms—here the relevant O atoms are O3 and O6.

(2) B layer octahedral sheet thickness: $(\Delta z_2)c\sin\beta$, where Δz_2 is the *largest* difference between z coordinates of O atoms of the B layer—here between O6 O atoms for which $\Delta z_2 = 1–2z$.

(3) 2:1 layer thickness: $(\Delta z_3)c\sin\beta$, where Δz_3 is the *largest* difference between z coordinates of O atoms of the basal-oxygen sheets—here between O3 O atoms, for which $\Delta z_3 = 2\ z$ (i.e., O3 at $\pm z$).

Metric relations between the polyhedral sheets of brucite and chlorite are: $a_{chl} \approx 2a_{bru}\cos 30°$, and $b_{chl} \approx 3a_{bru}$. Nearest O1-O4 distances in clinochlore (i.e., parallel to **b** of brucite) decrease by 0.063(7) Å, O1-O1 distances (parallel to **a** of brucite) decrease by 0.061(7) Å. For brucite over the same pressure range the corresponding contraction of a is 0.065(5) Å (Parise et al. 1994). Figure 6 compares the in-plane compressions of the polyhedral sheets of brucite [$Mg(OH)_2$ and $Mg(OD)_2$] and clinochlore, based upon the metric identities given above. It is evident that all trends are essentially parallel, indicating that the in-plane compressibilities of brucite and clinochlore are essentially the same. As with micas, the tetrahedral sheets of chlorite are expected to accommodate in-plane compression of the octahedral sheet by small rotations, although these could not be discerned, within error, from the refinements. No out-

TABLE 2. Atom coordinates and isotropic displacement parameters (Å²)

	0 GPa	1.2 GPa	2.5 GPa	4.7 GPa
		M2*		
y	0.353(2)	0.351(1)	0.352(2)	0.353(2)
U_{iso}	0.008(2)	0.010(2)	0.008(2)	0.007(2)
		M3*		
y	0.160(2)	0.168(2)	0.163(2)	0.175(2)
U_{iso}	0.015(2)	0.015(2)	0.015(2)	0.015(2)
		T		
x	0.224(5)	0.233(5)	0.219(4)	0.228(4)
y	0.166(3)	0.162(2)	0.161(2)	0.158(2)
z	0.193(1)	0.195(1)	0.198(1)	0.201(1)
U_{iso}	0.018(2)	0.016(2)	0.011(2)	0.006(2)
		O1		
x	0.185(5)	0.202(3)	0.191(3)	0.196(3)
y	0.172(2)	0.173(1)	0.171(1)	0.174(1)
z	0.080(1)	0.081(1)	0.080(1)	0.080(1)
U_{iso}	0.015(2)	0.008(2)	0.009(2)	0.007(2)
		O2		
x	0.228(5)	0.210(4)	0.207(3)	0.204(3)
z	0.234(2)	0.230(2)	0.233(1)	0.229(1)
U_{iso}	0.023(6)	0.020(5)	0.013(4)	0.010(3)
		O3		
x	0.509(4)	0.516(4)	0.516(3)	0.533(4)
y	0.220(2)	0.221(2)	0.216(2)	0.210(2)
z	0.231(1)	0.235(1)	0.234(1)	0.234(1)
U_{iso}	0.038(5)	0.040(5)	0.032(4)	0.035(4)
		O4		
x	0.181(5)	0.176(4)	0.175(3)	0.177(4)
z	0.068(1)	0.068(1)	0.071(1)	0.069(1)
U_{iso}	0.013(4)	0.012(3)	0.004(2)	0.004(2)
		O5		
x	0.168(6)	0.176(5)	0.172(5)	0.177(3)
z	0.435(2)	0.433(2)	0.436(2)	0.432(1)
U_{iso}	0.026(6)	0.027(5)	0.043(7)	0.007(3)
		O6		
x	0.135(4)	0.135(4)	0.134(3)	0.130(4)
y	0.337(2)	0.339(2)	0.336(1)	0.324(2)
z	0.430(1)	0.432(1)	0.430(1)	0.432(1)
U_{iso}	0.017(2)	0.016(2)	0.014(2)	0.026(3)
		D1		
x	0.200(8)	0.221(9)	0.239(7)	0.199(8)
z	0.142(2)	0.141(2)	0.145(1)	0.150(2)
U_{iso}	0.072(7)	0.069(5)	0.064(6)	0.074(7)
		D2		
x	0.120(10)	0.123(6)	0.099(7)	0.090(5)
z	0.371(2)	0.369(1)	0.374(2)	0.372(2)
U_{iso}	0.055(8)	0.039(4)	0.071(9)	0.039(5)
		D3		
x	0.117(10)	0.109(9)	0.126(6)	0.063(5)
y	0.320(4)	0.324(4)	0.322(3)	0.344(3)
z	0.358(2)	0.360(2)	0.358(1)	0.355(2)
U_{iso}	0.107(8)	0.118(8)	0.101(7)	0.099(8)

Notes:
M1 = 0 0 0.
M2 = 0 y 0.
M3 = 0 y ½.
M4 = 0 ½ ½.
O2, O5, D2: y = 0.
O4, D1: y = ½.
*U_{iso} of M1 set equal to U_{iso} of M2; U_{iso} of M4 set equal to U_{iso} of M3.
Cation-site occupancies: M1 = M2 = M3 = Mg, M4 = Al, T = 0.75 Si + 0.25 Al.

TABLE 3. Thicknesses (Å) of structural layers in clinochlore as a function of pressure

	0 GPa	1.2 GPa	2.5 GPa	4.7 GPa	Δ (0 to 4.7 GPa)
d (001)	14.304(2)	14.200(2)	14.117(2)	14.000(2)	–0.30(2)
Octa (B)	1.99(2)	1.98(2)	2.01(1)	1.97(2)	–0.02(2)
Interlayer*	2.83(2)	2.78(2)	2.75(2)	2.73(2)	–0.10(2)
2:1 layer	6.65(3)	6.67(3)	6.60(2)	6.57(3)	–0.08(3)
Tetrahedral*	2.22(2)	2.21(2)	2.17(2)	2.17(2)	–0.05(2)
Octa (2:1)	2.21(2)	2.26(2)	2.26(1)	2.22(2)	+0.01(2)

* Single layer thickness.

TABLE 4. Oxygen-deuterium bond distances (Å)

	0 GPa	1.2 GPa	2.5 GPa	4.7 GPa
	Restraint ON			
O4-D1	1.01(2)	1.01(3)	1.04(3)	1.03(3)
O5-D2	0.93(2)	0.92(3)	0.92(3)	0.94(3)
O6-D3	1.01(2)	1.00(2)	1.02(3)	1.04(2)
O2···D2	2.03(3)	2.07(3)	2.09(3)	2.11(4)
O3···D3	1.91(2)	1.87(2)	1.84(2)	1.79(2)
	Restraint OFF			
O4-D1	1.06(2)	1.05(3)	1.06(3)	1.13(3)
O5-D2	0.93(2)	0.93(3)	0.92(3)	0.91(3)
O6-D3	1.05(1)	1.03(2)	1.03(3)	1.10(2)
O2···D2	2.16(3)	2.11(4)	2.15(4)	2.18(4)
O3···D3	1.88(2)	1.85(2)	1.83(2)	1.77(2)

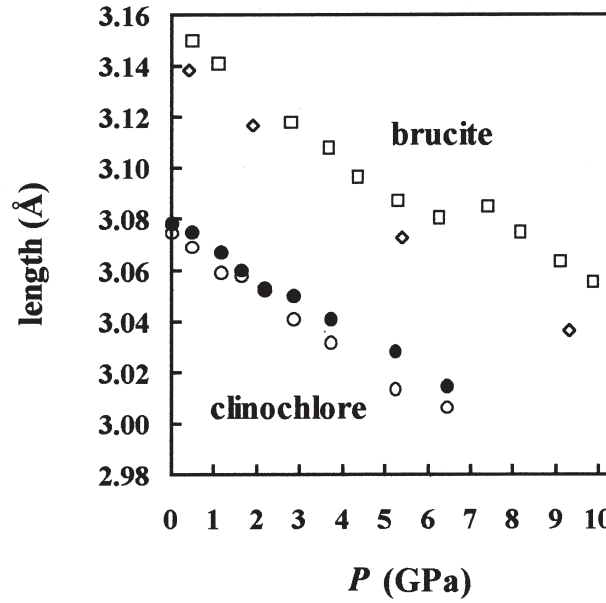

FIGURE 6. Comparison of the in-plane compression of the polyhedral sheets of clinochlore and brucite. Black and white circles refer to clinochlore normalized to the brucite *a* parameter: $a_{clinochlore}/2\cos30°$ (black) and $^1/_3\ b_{clinochlore}$ (white). Squares and diamonds refer to brucite data of Catti et al. (1995) for $Mg(OH)_2$ and Parise et al. (1994) for $Mg(OD)_2$, respectively.

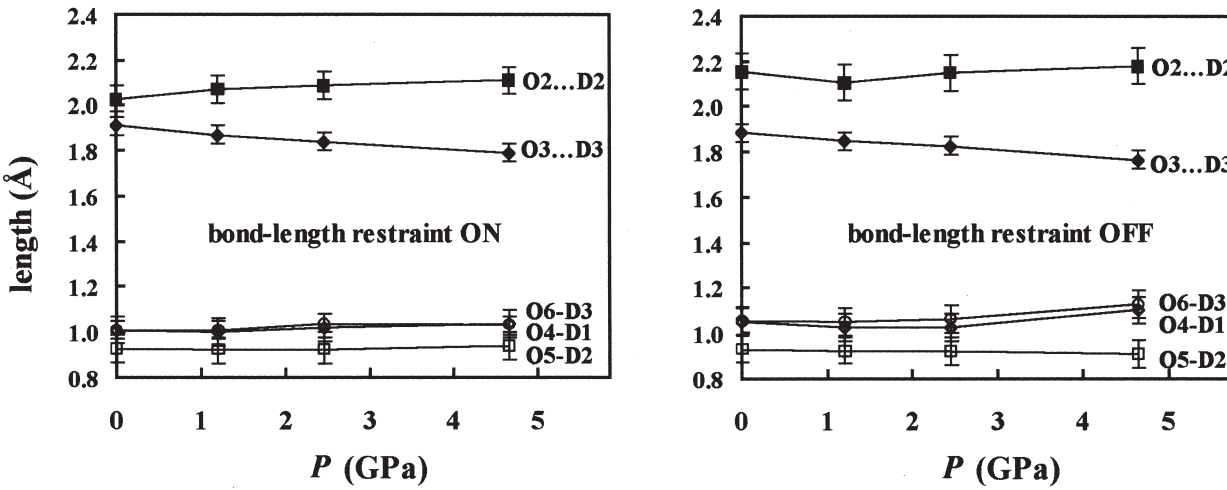

FIGURE 7. Hydroxyl and hydrogen-bond distances in clinochlore at 0, 1.2, 2.5, and 4.7 GPa, calculated with and without the soft restraint on O-D bond-lengths (see text). In both cases the O3···D3 hydrogen bond length shows the same linear decrease with increasing pressure.

of-plane buckling of the tetrahedral sheet was discernible. The very similar in-plane compressional behavior of the polyhedral sheets of brucite and clinochlore implies that the big difference between the bulk moduli of these minerals is due almost solely to their different compressibilities normal to the structural layering.

The thicknesses, as defined above, of the octahedral sheet of the B layer, the 2:1 layer and the interlayer as functions of pressure from 0 to 4.7 GPa are given in Table 3. Also shown are the thickness variations of the tetrahedral sheet and octahedral sheet of the 2:1 layer. Basal O atoms of the 2:1 layer are coplanar. We note that the interlayer thickness at 0 GPa calculated using O6 gives a thickness of 2.83(2) Å, which is tolerably close to that determined for natural Mg-rich clinochlore (2.79 Å) by Joswig et al. (1989). Some interesting trends are apparent from Table 3. The *d*(001), interlayer, and tetrahedral-layer spacings decrease with increasing pressure. The octahedral sheets are uncompressed, as is also found for brucite (Parise et al. 1994). The *d*(001) spacing decreases by 0.30 Å. The interlayer undergoes a steady compression from 2.83(2) Å at 0 GPa to 2.73(2) Å at 4.7 GPa. Interestingly, the contractions of the 2:1 layer (0.08 Å) and the interlayer (0.10 Å) over this pressure range are com-

parable; structurally the interlayer is as robust in compression as the 2:1 layer. The interlayer of brucite compresses by 0.2 Å over a similar pressure range (Parise et al. 1994); therefore the interlayer of clinochlore is twice as stiff as that of brucite. Clearly, the difference between their hydrogen-bonding topologies has a significant effect upon compressibility.

In passing we note that talc, with a vacant interlayer and no interlayer hydrogen bonding, is about twice as compressible [$K_0 = 42(1)$ GPa, $K_0' = 6.5(4)$: Pawley et al. 1995] as clinochlore. The difference between having interlayer hydrogen bonds and not is, therefore, very significant.

Hydrogen bonding

*C*2/*m* clinochlore has three non-equivalent hydrogen atoms: H1 is bonded to O4 of the octahedral sheet of the 2:1 layer; and H2 and H3 are bonded to O5 and O6 of the B layer, respectively. The O5-H2 hydroxyl lies within the mirror plane in a *trans* configuration relative to the Al cation, whereas O6-H3 lies off the mirror in *cis* configuration. There are two different hydrogen bonds, O2···D2 and O3···D3. Deuteron positions were easily seen in Fourier maps. The responses of the O-D and O···D bonds to pressure are shown in Table 4 and Figure 7. Refinements in which the soft restraint on O-D bond-lengths was used (ON) and was not used (OFF) give comparable results. In both cases there is a well-defined linear decrease in the O3···D3 hydrogen-bond distance from 1.91(3) to 1.77(3) Å. Indeed, at 1.77 Å (4.7 GPa) O3···D3 is a short hydrogen bond. In contrast, the O2···D2 hydrogen-bond distance is, within error, invariant. O5-D2 and O6-D3 bonds show little change in length with increasing pressure, although the "restraint OFF" result has a noticeable increase (to ~1.1 Å) in both O-D distances at 4.7 GPa. Within error, the O4-D1 bond-length does not change with pressure. The O6-D3···O3 angle, which is sensitive to interlayer contraction, decreases from ~170° at 0–1.2 GPa to ~155° at 4.7 GPa (Fig. 8). This angular reduction is consistent with the observed interlayer contraction.

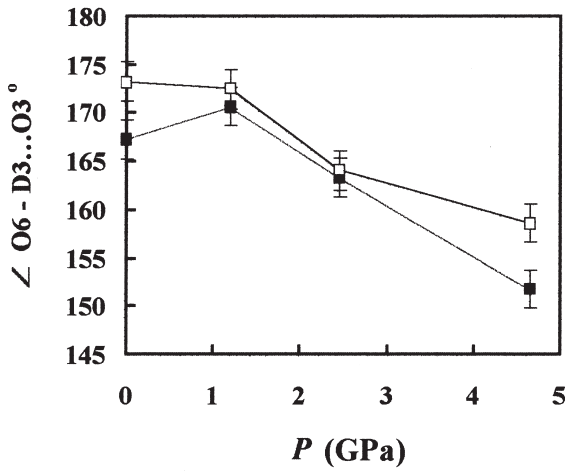

FIGURE 8. The O6-D3···O3 bond-angle as a function of pressure, with and without the soft restraint on O-D bond lengths (open and filled squares, respectively).

The main conclusions from this study are:

(1) The interlayer and 2:1 layer have similar compressibilities. Compression of the 2:1 layer involves only the tetrahedral sheets.

(2) The octahedral sheets in clinochlore and brucite are essentially uncompressed normal to the layering.

(3) The clinochlore interlayer is twice as stiff as that of brucite.

(4) The difference in brucite and clinochlore bulk moduli is due, in equal part, to the presence of a 2:1 layer *and* the different hydrogen-bonding topologies of the interlayer. In-plane compressions of clinochlore and brucite are very similar.

(5) Hydrogen-bonding topology can have a major effect upon mineral compressibilities.

ACKNOWLEDGMENTS

M.D.W. thanks the Natural Environment Research Council for support through grant GR9/03560. We thank Kevin Knight for advice on refinement strategies and Duncan Francis for technical support.

REFERENCES CITED

Bailey, S.W. (1988) Chlorites: structures and crystal chemistry. Reviews in Mineralogy, 19, 347–398.

Baker, J. and Holland, T.J.B. (1996) Experimental reversal of chlorite compositions in divariant $MgO+Al_2O_3+SiO_2+H_2O$ assemblages. American Mineralogist, 81, 676–684.

Bevington, P.R. (1969) Data reduction and error analysis for the physical sciences, p. 336. McGraw-Hill.

Catti, M., Ferraris, G., Hull, S., and Pavese, A. (1995) Static compression and H disorder in brucite, $Mg(OH)_2$, to 11 GPa: a powder neutron diffraction study. Physics and Chemistry of Minerals, 22, 200–206.

Circone, S., Navrotsky, A., Kirkpatrick, R.J., and Graham, C.M. (1991) Substitution of $^{[6,4]}Al$ in phlogopite: mica characterization, unit-cell variation, ^{27}Al and ^{29}Si MAS NMR spectroscopy, and Al-Si distribution in the tetrahedral sheet. American Mineralogist, 79, 1485–1501.

Decker, D.L. (1971) High-pressure equation of state for NaCl, KCl and CsCl. Journal of Applied Physics, 42, 3239–3244.

Hazen, R.M. and Finger, L.W. (1978) The crystal structures and compressibilities of layer minerals at high pressure; II, phlogopite and chlorite. American Mineralogist, 63, 293–296.

Herrero, C.P., Sanz. J., and Serratosa, J.M. (1987) Tetrahedral cation ordering in layer silicates by ^{29}Si MAS NMR spectroscopy. Solid State Communications, 53, 151–154.

Jenkins, D.M. (1981) Phase relations of hydrous peridotites in the system $CaO-MgO-Al_2O_3-SiO_2-H_2O$. Contributions to Mineralogy and Petrology, 77, 166–176.

Jenkins, D.M. and Chernosky, J.V. (1986) Phase equilibria and crystallochemical properties of Mg-chlorite. American Mineralogist, 71, 924–936.

Joswig, W., Fuess, H., and Mason, S.A. (1989) Neutron diffraction study of a one-layer monoclinic chlorite. Clays and Clay Minerals, 37, 511–514.

Larson, A.C. and Von Dreele, R.B. (1994) GSAS general structure analysis system manual. LAUR 86-748, Los Alamos National Laboratory.

Nelmes, R.J., Loveday, J.S., Wilson, R.M., Besson, J.M., Klotz, S. Hamel, G., and Hull, S. (1993) Structure studies at high pressure using neutron powder diffraction. Transactions of the American Crystallographic Association, 29, 19–27.

Parise, J.B., Leinenweber, K., Weidner, D.J., Tan, K., and Von Dreele, R.B. (1994) Pressure-induced H bonding: Neutron diffraction study of brucite, $Mg(OD)_2$, to 9.3 GPa. American Mineralogist, 79, 193–196.

Pawley, A.R., Redfern, S.A.T., and Wood, B.J. (1995) Thermal expansivities and compressibilities of hydrous phases in the system $MgO-SiO_2-H_2O$: talc, Phase A and 10-Å phase. Contributions to Mineralogy and Petrology, 122, 301–307.

Peacock, S.M. (1990) Fluid processes in subduction zones. Science, 248, 329–337.

Rule, A.C. and Bailey, S.W. (1987) Refinement of the crystal structure of monoclinic ferroan clinochlore. Clays and Clay Minerals, 35, 129–138.

Smyth, J.R., Darby Dyar, M., May, H.M., Bricker, O.P., and Acker, J.G. (1997) Crystal structure refinement and Mössbauer spectroscopy of an ordered, triclinic clinochlore. Clays and Clay Minerals, 45, 544–550.

Welch, M.D., Barras, J., and Klinowski, J. (1995) A multinuclear NMR study of clinochlore. American Mineralogist, 80, 441–447.

MANUSCRIPT RECEIVED NOVEMBER 30, 2000
MANUSCRIPT ACCEPTED JULY 5, 2001
MANUSCRIPT HANDLED BY YINGWEI FEI